




Article

Indocyanine Green Loaded Modified Mesoporous Silica Nanoparticles as an Effective Photothermal Nanoplatfrom

Yiyu Wang ^{1,2,*} , Chunqing Niu ^{1,2}, Sisi Fan ^{1,2}, Yuwei Li ^{1,2}, Xiang Li ^{1,2}, Yujun Dai ^{1,2}, Jian Shi ³ and Xinyu Wang ^{4,5,*}

¹ Hubei Province Research Center of Engineering Technology for Utilization of Botanical Functional Ingredients, Hubei Engineering University, Xiaogan 432000, China; niuchunqing@hotmail.com (C.N.); fss18186130620@hotmail.com (S.F.); lyw0213@hotmail.com (Y.L.); lixiang980@hotmail.com (X.L.); dyj5925@hbeu.edu.cn (Y.D.)

² Hubei Key Laboratory of Quality Control of Characteristic Fruits and Vegetables, Hubei Engineering University, Xiaogan 432000, China

³ Department of Machine Intelligence and Systems Engineering, Faculty of Systems Science and Technology, Akita Prefectural University, Akita 015-0055, Japan; shij@akita-pu.ac.jp

⁴ State Key Laboratory of Advanced Technology for Materials Synthesis and Processing, Wuhan University of Technology, Wuhan 430070, China

⁵ Biomedical Materials and Engineering Research Center of Hubei Province, Wuhan University of Technology, Wuhan 430070, China

* Correspondence: wangyiyu@hbeu.edu.cn (Y.W.); wangxinyu@whut.edu.cn (X.W.)

Received: 7 June 2020; Accepted: 3 July 2020; Published: 6 July 2020



Abstract: Photothermal therapy possesses great advantages for the treatment of drug-resistant tumors. Herein, Near Infrared (NIR)-triggered photothermal nanoparticles were developed through loading indocyanine green (ICG), a kind of NIR dye, into amino group-modified silica nanoparticles (SiO₂-NH₂ NPs). SiO₂-NH₂ NPs were prepared with immobilization of the amino groups into the framework of silica nanoparticles (SiO₂ NPs) by employing (3-aminopropyl)-triethoxysilane (APTES). Before and after the modification of the amino group, the particle sizes of SiO₂ NPs showed similar value, around 100 nm. ICG was further adsorbed into SiO₂-NH₂ NPs by electrostatic attraction to enable SiO₂-NH₂@ICG NPs as a kind of photothermal agent. The loading rate of ICG to SiO₂-NH₂ was greatly increased compared to unmodified SiO₂, and the stability of ICG was also improved. Moreover, the SiO₂-NH₂@ICG NPs exhibited efficient photothermal effects due to ICG transforming laser power into local heat through the connected ICG, when NIR laser irradiation turned on for a couple of minutes. Finally, the in vitro antitumor efficacy of SiO₂-NH₂@ICG NPs was investigated by recording cell proliferation rate and further chronicled the apoptotic morphology evidence by a Calcein-AM/PI fluorescent staining assay, indicating the efficient photothermal targeted therapy for the HepG2 tumor cells.

Keywords: mesoporous silica nanoparticles; indocyanine green; NIR-triggered; photothermal effect; tumor cells

1. Introduction

Liver cancer is one of the most common cancers in the world, which is threatening human health and life. In the past few decades, the number of liver cancer patients significantly increased; liver cancer contains hepatocellular carcinoma (HCC) and intrahepatic cholangiocarcinoma (ICC) [1], and HCC patients are often diagnosed at late stages due to its asymptomatic features. Current diagnostic

approaches, like ultrasound and α -fetoprotein, are expensive and lack sensitivity in HCC detection [2]. It is necessary to find new systematic therapeutic modalities for diagnosis and therapy of liver cancer. The common cancer therapeutics, such as transarterial chemoembolization, surgical excision of hepatocellular carcinoma and radiofrequency ablation, increase the survival rate of liver cancer patients [3]. However, we still need to study a new therapeutic platform with fewer side effects to break through the bottleneck of traditional therapeutics. Photothermal therapy (PTT) is a minimally invasive technical method for cancers, which can transform the light energy into thermal energy under light irradiation with the help of photoabsorbers [4–6]. As is known to all that all light wavelengths can penetrate the skin in different depths, however, Near Infrared (NIR) light can usually penetrate deeper than other wavelengths; therefore, it is more common to use photosensitive nanoparticles *in vivo*, causing less damage to healthy tissues [7]. Hence, NIR light-triggered photothermal nanoagents have attracted much interest for PTT application. Recently, many photothermal nanoagents were developed for generating efficient thermal energy, such as metal nanoparticles, semiconductor nanoparticles (CuS), boron nitride nanosheets (BN)-polydopamine (PDA) immobilized poly (p-phenylene benzobisoxazole) (PBO) fibers, nanohybrid and carbon-based materials (carbon nanotubes or graphenes) [8–14].

It is well known to us that various dyes have different and unique light responsiveness and light adsorption, therefore, those dyes can also be applied to various fields [15,16]. Indocyanine green (ICG) is a low toxicity and injectable NIR organic dye; it is also approved by the US Food and Drug Administration (FDA) for clinical use [17,18]. At present, ICG is widely used in clinical diagnosis such as optical angiography [19] and guiding sentinel node biopsy [20]. However, as a small molecular photothermal agent, more extensive applications of ICG are rather limited because of the following drawbacks. ICG has a low fluorescence quantum yield in aqueous solutions because of self-quenching [21] and it cannot be fully used in physiological aqueous conditions [22]. Furthermore, ICG binds to plasma proteins nonspecifically, such as albumin, globulins, and lipoproteins, which can be quickly removed from the circulatory system by the action of the liver, so the initial half-life of pure ICG is only about 3–4 min [23]. To overcome such drawbacks, recently, various types of nanoparticles were adopted for improving the stability of ICG, such as FA ICG-PLGA-lipid NPs, PC-FA/ICG/DOX nanocarriers, MSN-TA-ICG, ICG@HMSNPs, and UCNP@mSiO₂-ICG nanopatform [24–31]. It was reported that mesoporous silica nanoparticles (SiO₂ NPs), with ordered mesoporous structure and well-defined surface properties for modification, provided great targeting versatility [32–34]. In addition, SiO₂ NPs have been considered as an excellent ICG carrier due to ease of synthesis, high surface area and pore volume, tunability of their pore size and good stability [35]. Additionally, SiO₂ has been listed by the US Food and Drug Administration (FDA) as ‘generally recognized as safe’ and is considered to be biocompatible [36,37]. Although PTT and combined PTT and chemotherapy have been developed, the challenge is still ongoing. Therefore, the facile ICG loading to SiO₂ NPs methods with safe performance need to be further studied for PTT application.

Herein, we designed and fabricated NIR-triggered photothermal NPs by loading the photothermal agent ICG into the amino functional silica nanoparticles (SiO₂-NH₂ NPs). SiO₂-NH₂ NPs were prepared through an improved base-catalyzed sol–gel method. The characterization of the modified nanoparticles was studied. Then, photothermal ability and ICG stability performance were analyzed. Finally, hemolysis, *in vitro* cytotoxicity and NIR-triggered phototoxicity, for killing HepG2 tumor cells of the modified nanoparticles, also were fully evaluated.

2. Results and Discussion

2.1. Preparation and Characterization

The synthesis procedure of amino-modified SiO₂ NPs loading with ICG is schematically elucidated in Figure 1. Firstly, in order to endow amino groups into the framework of SiO₂ NPs, the modified SiO₂ NPs were prepared by adding a small amount of aminosilane agent (APTES) during the process of SiO₂ formation using the sol–gel method. The positively charged SiO₂-NH₂ could be later used for

static-adsorbing negatively charged ICG molecules. Afterward, ICG was loaded into the SiO₂-NH₂ NPs. In this study, ICG was selected as an NIR responsive photothermal agent because the ICG molecule has demonstrated its photothermal effect in terms of its high optical absorbance in the NIR region [27] and it can be used as heat donor for fabrication of NIR-responsive nanoparticle vehicles. We denoted this product as SiO₂-NH₂@ICG NPs. The typical outer morphology and inner structure of the SiO₂ and SiO₂-NH₂ were characterized by transmission electron microscope (TEM), as shown in Figure 2. The particle size was calculated by Image J software and particle size distributions are given as insets in Figure 2c,d. These TEM images show both of SiO₂ and SiO₂-NH₂ NPs have spherical particles with uniform size. The average diameter of SiO₂ measured from TEM images is 108 ± 6 nm, while the diameter of SiO₂-NH₂ is around 102 ± 13 nm. The reason for the reduction in particle size of NPs after amino modification may be that the addition of APTES in the final 2 h during the process of SiO₂-NH₂ formation had a tiny impact on the deposition of silica. The mesoporous trait of the SiO₂ is also apparently observed in the SiO₂-NH₂, as shown in Figure 2b, and this trait offers the opportunity for the NPs to serve as general drug vehicles. Compared to NPs' unloaded ICG, the TEM images of NPs after loading ICG do not show any changes in terms of particle size and mesoporous structure inside (Figure S1).

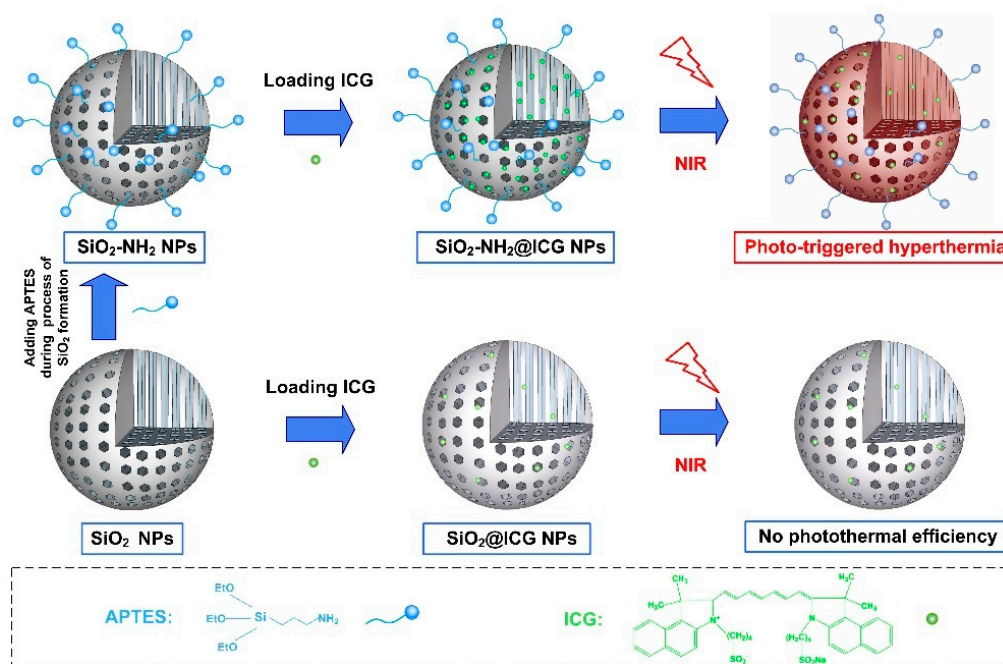


Figure 1. Schematic view of the synthesis procedure of amino group modified SiO₂ NPs loading with ICG and the NIR-triggered hyperthermia performance.

The surface area and the inner pore size characteristic of the NPs were analyzed by the N₂ adsorption/desorption technique, as shown in Figure 3a. SiO₂-NH₂ exhibits a reversible type IV isotherm, which is one of the main characteristics of mesoporous materials. The total surface area of SiO₂-NH₂ was 426.30 m²/g calculated by the (Brunauer–Emmet–Teller) BET model, and the average mesoporous pore diameter of the SiO₂-NH₂ was 3.12 nm, which was calculated from the adsorption branch of the isotherm using the Barrett–Joyner–Halenda (BJH) model. After loading ICG, the total surface area slightly decreased to 328.58 m²/g and the pore diameter declined to 2.86 nm as well. The result implied this SiO₂-NH₂ could be employed as a drug carrier with high drug payload, and reduction in surface area and pore diameter illustrated that ICG can enter the internal channels of SiO₂-NH₂ NPs. The DLS results were shown in Figure 3b, which clearly showed both SiO₂ and SiO₂-NH₂ NPs prepared by the sol–gel method exhibited a narrow hydrodynamic particle size

distribution. The average hydrodynamic particle sizes of SiO₂ and SiO₂-NH₂ NPs were around 206 ± 15 and 187 ± 10 nm in D.I. water.

The DLS particle size was calculated from the mean data of intensity distribution, which are larger than tested by TEM. The reason for this difference may be ascribed to the hydrodynamic diameter in the hydrated state or aggregation. The results of zeta potential analysis data are shown in Figure 3c. The APTES functionalization containing amino groups changes the zeta potential of the SiO₂ NPs from a negative to a positive value. The zeta potential of SiO₂, SiO₂-NH₂, SiO₂-NH₂@ICG and SiO₂-NH₂@ICG were about -32.95, 31.29, -32.20 and 30.79 mV, respectively. The surface potential of SiO₂ was successfully changed by adding APTES during the process of SiO₂ fabrication. ICG loading had little effect on the surface potential of both SiO₂ and SiO₂-NH₂ NPs.

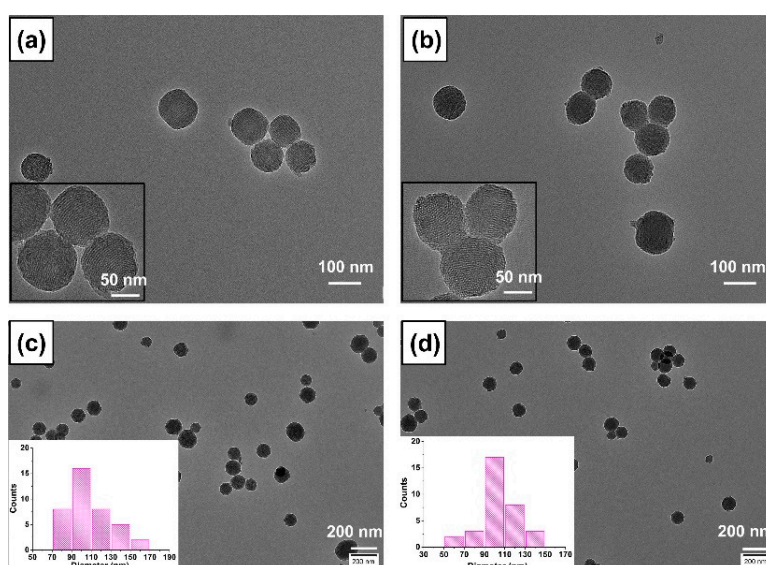


Figure 2. TEM images of (a) SiO₂ NPs (amplified image), (b) SiO₂-NH₂ NPs (amplified image), (c) SiO₂ NPs (the particle size distribution as an inset), (d) SiO₂-NH₂ NPs (the particle size distribution as an inset). The histograms were generated by measuring the diameter of about 40 particles from the TEM images.

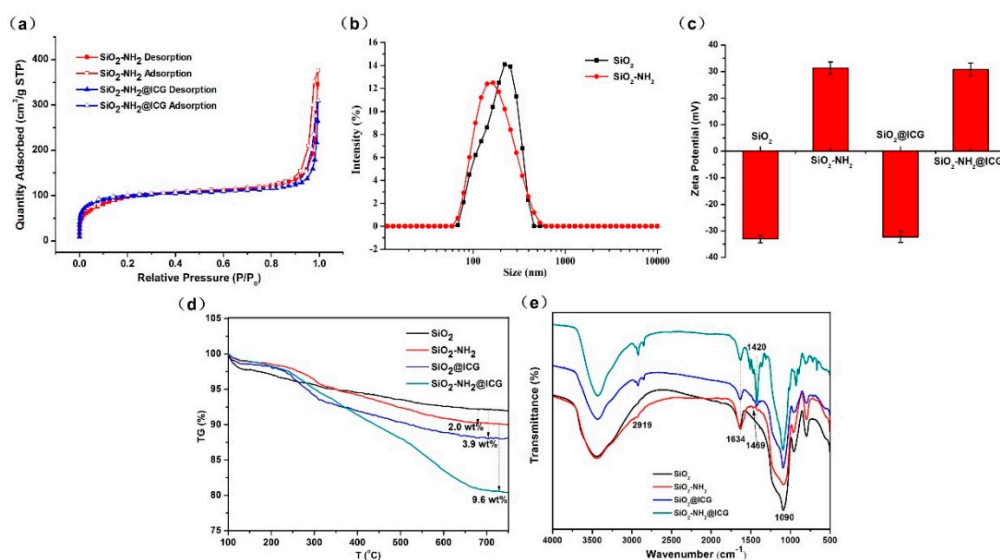


Figure 3. (a) N₂ adsorption/desorption isotherms of the SiO₂-NH₂ and SiO₂-NH₂@ICG NPs; (b) DLS measurement of the size distribution of SiO₂ and SiO₂-NH₂ NPs; (c) zeta potentials of SiO₂, SiO₂-NH₂, SiO₂@ICG and SiO₂-NH₂@ICG; (d) TG curves of SiO₂, SiO₂-NH₂, SiO₂@ICG and SiO₂-NH₂@ICG NPs; (e) Fourier-transform infrared (FTIR) spectra of SiO₂, SiO₂-NH₂, SiO₂@ICG and SiO₂-NH₂@ICG NPs.

The thermal stability and modification by APTES were examined by TG analysis, as shown in Figure 3d. These NPs showed reliably high stability. Slight weight loss between 100 and 750 °C can be observed, which can mainly be due to the loss of water and hydroxyl groups physically adsorbed in SiO₂. It could be calculated from the TG curves that the grafted amino group onto SiO₂ accounted for 2.0 wt%. Furthermore, the weight of ICG loaded into the SiO₂ and SiO₂-NH₂ were measured by TG analysis, and the ICG weight loss from SiO₂@ICG was calculated to be 3.9 wt%, which is significantly less than 9.6 wt% from SiO₂-NH₂@ICG, indicating that ICG loading capacity of SiO₂-NH₂ was significantly higher than that of SiO₂. The FTIR spectra were presented in Figure 3e. The FTIR spectra of pure ICG were also recorded in the SI Figure S2. As shown in Figure 3e, for SiO₂ (black curve), the peaks around 1090 and 800 cm⁻¹ are assigned to characteristic absorption peaks of silica. The absorption peak at 3400 cm⁻¹ can be attributed to the stretching of -OH and the peaks around 1634 cm⁻¹ belong to the bending of H-O-H [38]. The red curve of Figure 3e represents SiO₂-NH₂; comparing to curve of SiO₂, a new weak absorption peak at 1469 cm⁻¹ appeared, which can be ascribed to characteristic absorption peaks of amino group in the modifier [39]. As can be seen from SiO₂@ICG (blue curve) and SiO₂-NH₂@ICG (green curve), new absorption peaks appeared at 2919 and 1420 cm⁻¹, assigned to characteristic peaks of ICG, indicating that the both SiO₂ and SiO₂-NH₂ NPs were successfully loaded with ICG. Moreover, these two absorption peaks were much stronger in the green curve, further confirming SiO₂-NH₂ possessed a higher loading rate for ICG.

2.2. Loading of ICG Molecules and Photothermal Effect

ICG were loaded into the SiO₂ and SiO₂-NH₂ NPs via small molecule free diffusion and intermolecular forces between ICG and functional groups of the NPs surface. The molecular weight of ICG is 548.63, which is small enough to load into the framework of SiO₂-NH₂ NPs [28]. ICG loading experiment results showed that the ICG loading efficiency (LE) of SiO₂ NPs was relatively low, only 21.60%, while the ICG LE of SiO₂-NH₂ NPs was significantly improved to 99.87% (Table S1). According to the previous reports [28], modified mesoporous silica with the TA group into the framework can adsorb more ICG by strong electrostatic attraction between sulfonic groups of ICG and amino groups of modified silica. SiO₂-NH₂ NPs showed obvious positive zeta potential due to amino modification, so SiO₂-NH₂ NPs can be employed as an ICG carrier with high loading amount. The ICG release rates from the SiO₂@ICG and SiO₂-NH₂@ICG in vitro were shown in the Figure 4a. Almost no premature ICG release from SiO₂@ICG was observed after 48h in PBS solution. In addition, the ICG release from SiO₂-NH₂@ICG was also relatively low, which finally reached 20.14% (pH = 7.0) after 24h and remained a stable value with extension of time. Under weak acid condition, ICG release was significantly reduced to 13.80% (pH = 6.2), because pH value affects the electrostatic interaction between ICG and the NPs [28]. The lower ICG release rate in vitro indicated that ICG loaded into nanoparticles could be stable for use as a photothermal agent.

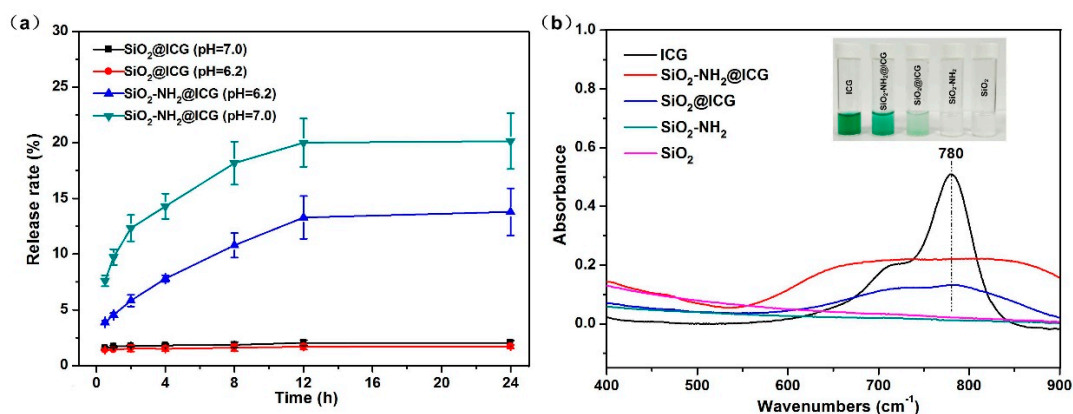


Figure 4. (a) Release behavior of ICG from the SiO₂@ICG NPs and SiO₂-NH₂@ICG NPs in PBS (pH = 6.2 or pH = 7.4); (b) UV-vis spectra of ICG, SiO₂-NH₂@ICG, SiO₂@ICG, SiO₂-NH₂ and SiO₂ NPs in aqueous solution (ICG concentration is 5 µg/mL, NPs concentration is 500 µg/mL).

UV-vis spectra of the obtained drug loaded NPs and the pure NPs were monitored through the UV-vis analyzer, as shown in Figure 4b. The absorption spectrum of ICG showed a clear characteristic peak around 780 nm. In addition, the spectra of ICG loaded NPs in an aqueous solution showed relatively broader and lower between 600 and 950 nm compared with that of free ICG, which meant that the ICG molecules were actually inside the NPs [40]. The absorption spectrum of SiO₂-NH₂@ICG was obviously stronger than that of SiO₂@ICG, which confirmed higher ICG loading capacity of SiO₂-NH₂ NPs once again. The broader absorption band of NPs might be attributed to the polaronic- π^* transitions because of the electrostatic interaction between ICG molecules and the NPs [28,41,42].

As an NIR dye, the stability of ICG greatly affects its photothermal performance. Free ICG are labile in aqueous solution and are easily prone to degradation and destruction. However, the stability of ICG can be significantly improved by nanocarrier encapsulation. In this study, irradiation stability, thermal stability and long-term stability were measured, as shown in Figure 5a–c. When under irradiation of an NIR laser the first time, the temperature rise of ICG solution was evidently higher than that of the SiO₂-NH₂@ICG NPs group. The reason for this difference of temperature changes is that the peak absorbance of ICG in nanoparticle suspension was about half that of the free ICG solution, and this attenuation of absorbance can be responsible for the lower photothermal effect when the samples were irradiated for the first time. However, as the irradiation times increased, the temperature variation of ICG solution decreased obviously, while the NPs group remained the relatively stable photothermal efficiency compared to free ICG solution. After the third irradiation, the photothermal ability of the two groups were nearly equal. The irradiation stability results indicated that the photothermal ability of the SiO₂-NH₂@ICG NPs group was more stable after multiple irradiations, because free ICG suffer degradation and destruction when exposed to constant lights [43]. Figure 5b showed that the photothermal effect for both of samples were almost unchanged within 8 h at low temperature, while the photothermal effect decreased gradually with the extension of storage time at 40 °C, and the photothermal effect of ICG solution decreased more obviously. Therefore, low temperature was beneficial to maintain the photothermal efficiency for both of them, and free ICG became more unstable under high temperature conditions, but nanoparticles entrapped ICG was to establish its effectiveness in preserving ICG from thermal damage. Furthermore, after 15 days of storage at 4 °C (Figure 5c), photothermal efficiency of SiO₂-NH₂@ICG NPs had remained stable since the third day, while the photothermal efficiency of the ICG solution dropped continuously.

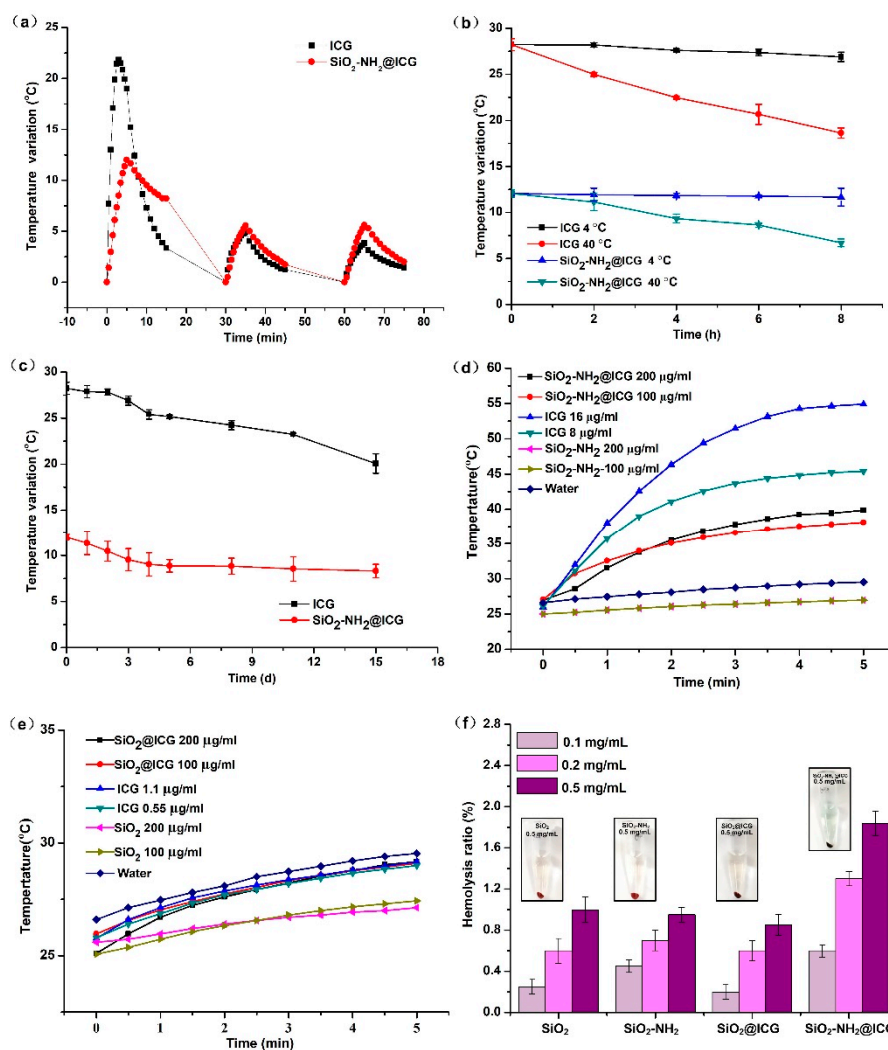


Figure 5. (a) Irradiation stability of SiO₂-NH₂@ICG. (b) Thermal stability of SiO₂-NH₂@ICG. (c) Long-term stability of SiO₂-NH₂@ICG. (d) Temperature elevation of SiO₂-NH₂@ICG NPs with different concentrations with exposure to NIR laser irradiation (808 nm, 1.5 W/cm²) for 5 min. DI water was used as a control. (e) Temperature elevation of SiO₂@ICG NPs with different concentrations with exposure to NIR laser irradiation (808 nm, 1.5 W/cm²) for 5 min. DI water was used as a control. (f) Hemolysis ratio of nanoparticles with different concentrations.

The photothermal effect of ICG, SiO₂-NH₂@ICG and SiO₂@ICG was investigated using D. I. water as a blank control. It can be observed from Figure 5d that the temperature of ICG solution increased fastest from 27 to 54 °C. However, temperature variation under NIR irradiation was approximately halved in the case of SiO₂-NH₂@ICG compared to free ICG. This may be due to the significantly lowered absorbance of SiO₂-NH₂@ICG in the NIR region. Besides, with the increasing ICG or SiO₂-NH₂@ICG concentration, the temperature rose much faster upon NIR irradiation. It can be seen from the Figure 5e that the photothermal efficiency of SiO₂@ICG was much lower under NIR irradiation. The different temperature increase in Figure 5d,e was due to the much less amount of ICG entrapped inside SiO₂ when the concentration of NPs was same. The hemolysis assays were used to evaluate the biocompatibility of these NPs. The results in Figure 5f showed that the maximum hemolysis ratio was at 1.84 ± 0.12% assigned to 0.5 mg/mL of SiO₂-NH₂@ICG NPs, indicating that the red blood cells are not compromised even at relatively high concentration (0.5 mg/mL). The hemolysis ratios of all groups were far less than 5%, which implied that they possessed good blood compatibility.

2.3. In Vitro Cytotoxicity and Phototoxicity Study

To intuitively evaluate the cytotoxicity of NPs aforementioned, Hoechst 33342 and the PI fluorescent staining method was used to confirm apoptosis and cell death. Figure 6a showed photomicrographs of HepG2 cells stained with Hoechst 33342 (blue) and PI (red) fluorescent dye after exposure to free ICG and different NPs groups for three days. Compared to the blank group, a similar number of normal cells were observed in the ICG, SiO₂-NH₂, and SiO₂-NH₂@ICG groups. Meanwhile, there were relatively higher dead cells observed in the SiO₂ and SiO₂@ICG groups, indicating that both SiO₂ and SiO₂@ICG NPs exhibited higher cytotoxicity than the other NPs.

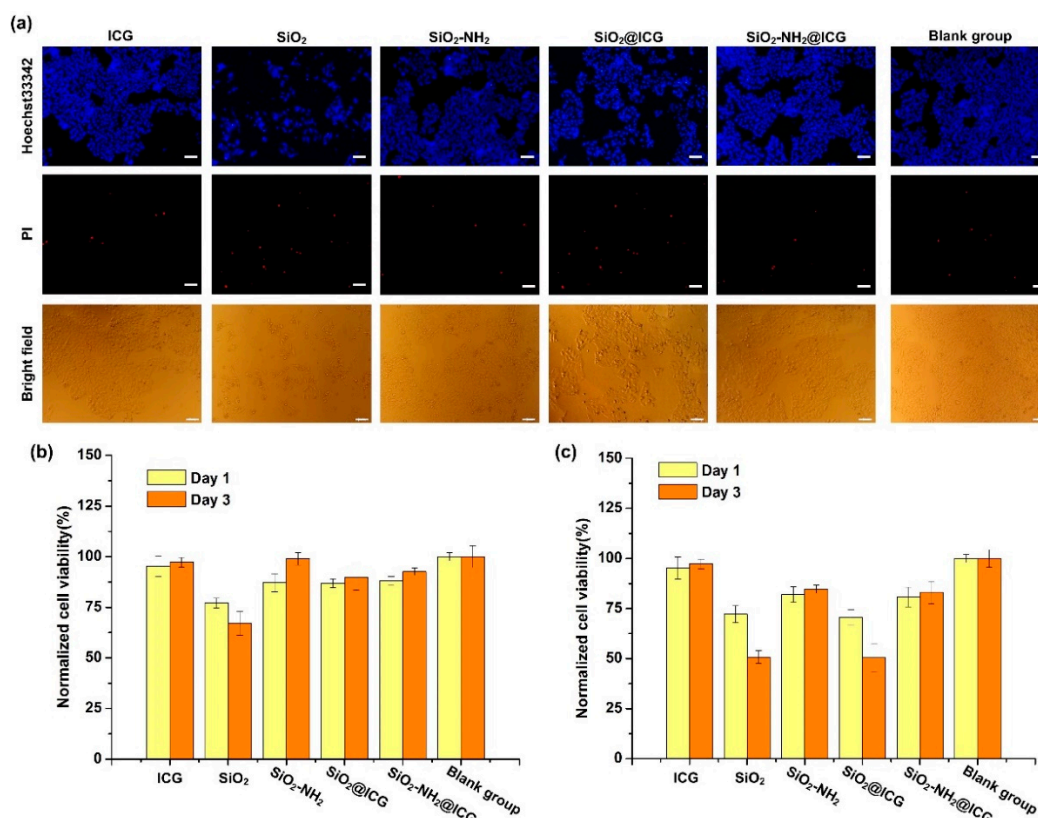


Figure 6. (a) The HepG2 cells treated with free ICG or different samples media after the 3-day culture were stained with Hoechst 33342 (blue) and PI (red) fluorescent dye (ICG concentration was fixed at 8 µg/mL), scale bars, 100 µm. (b) Viability of HepG2 cells on the first and third days after incubation with ICG (4 µg/mL) or different samples media (50 µg/mL) but without laser irradiation. (c) Viability of HepG2 cells on the first and third days after incubation with ICG (8 µg/mL) or different samples media (100 µg/mL) but without laser irradiation.

In order to further analyze the effect of NPs on cell apoptosis, Annexin V-FITC/PI staining assay was performed to confirm the apoptosis of HepG2 cells. The apoptosis of HepG2 cells exposure to SiO₂, SiO₂-NH₂, SiO₂@ICG, and SiO₂-NH₂@ICG without NIR treatment was investigated by Flow Cytometry, while cells co-incubated with normal medium and free ICG were used as controls (the concentration of ICG was fixed at 8 µg/mL). As shown in Figure S3 and Table S2 (Supporting Information), the cells treated different NPs did not display significant apoptosis, whereas the cells treated with SiO₂ exhibited relatively higher apoptosis rate, at 4.59%. The apoptosis rates of all groups were less than 5%, and negligible necrosis also was observed, which indicated free ICG and NPs obtained in this experiment cannot induce cell apoptosis. These results could be ascribed to the fine biocompatibility of unirradiated ICG and the superior cellular compatibility of SiO₂-NH₂.

The viability results of HepG2 cells exposure to the free ICG or NPs media with different concentrations were recorded in the Figure 6b,c. It can be seen from Figure 6b that the viability of

HepG2 cells incubation with NPs media at the 50 $\mu\text{g}/\text{mL}$ for one and three days were insignificant difference compared to the blank group, except in the SiO_2 group. A slight reduction in cell viability after incubation with SiO_2 for three days can be observed. Moreover, as the concentration of NPs rose to 100 $\mu\text{g}/\text{mL}$, viability of HepG2 cells incubation with NPs media declined at different levels. The $\text{SiO}_2\text{-NH}_2$ and $\text{SiO}_2\text{-NH}_2\text{@ICG}$ groups exhibited higher HepG2 cells proliferation compared with the SiO_2 and $\text{SiO}_2\text{@ICG}$ groups. Significantly reduced cell viability of 50% after incubation with SiO_2 and $\text{SiO}_2\text{@ICG}$ for three days was observed, indicating SiO_2 and $\text{SiO}_2\text{@ICG}$ showed the higher cytotoxicity to HepG2 cells. These results indicated that the $\text{SiO}_2\text{-NH}_2$ and $\text{SiO}_2\text{-NH}_2\text{@ICG}$ NPs with better cellular compatibility could promote HepG2 cell proliferation.

To evaluate the NIR responsive photothermal effect of $\text{SiO}_2\text{-NH}_2\text{@ICG}$ for killing HepG2 cells, Calcein-AM and PI fluorescent staining and MTT assay were applied to distinguish the live/dead cells and evaluate cells viability with or without NIR irradiation. Figure 7a showed there were no obvious dead cells that could be observed in the SiO_2 , $\text{SiO}_2\text{-NH}_2$, $\text{SiO}_2\text{@ICG}$ and blank group under NIR irradiation, suggesting that 808 nm NIR laser illumination with the output of 1.5 W cm^{-2} for 5 min was safe for the HepG2 cells, and $\text{SiO}_2\text{@ICG}$ had inefficient photothermal effect due to the low ICG loading rate, which cannot kill HepG2 cells. However, the cells incubated with $\text{SiO}_2\text{-NH}_2\text{@ICG}$ were induced to death obviously under NIR irradiation, indicating it possessed superior photothermal conversion ability that can kill HepG2 cells effectively.

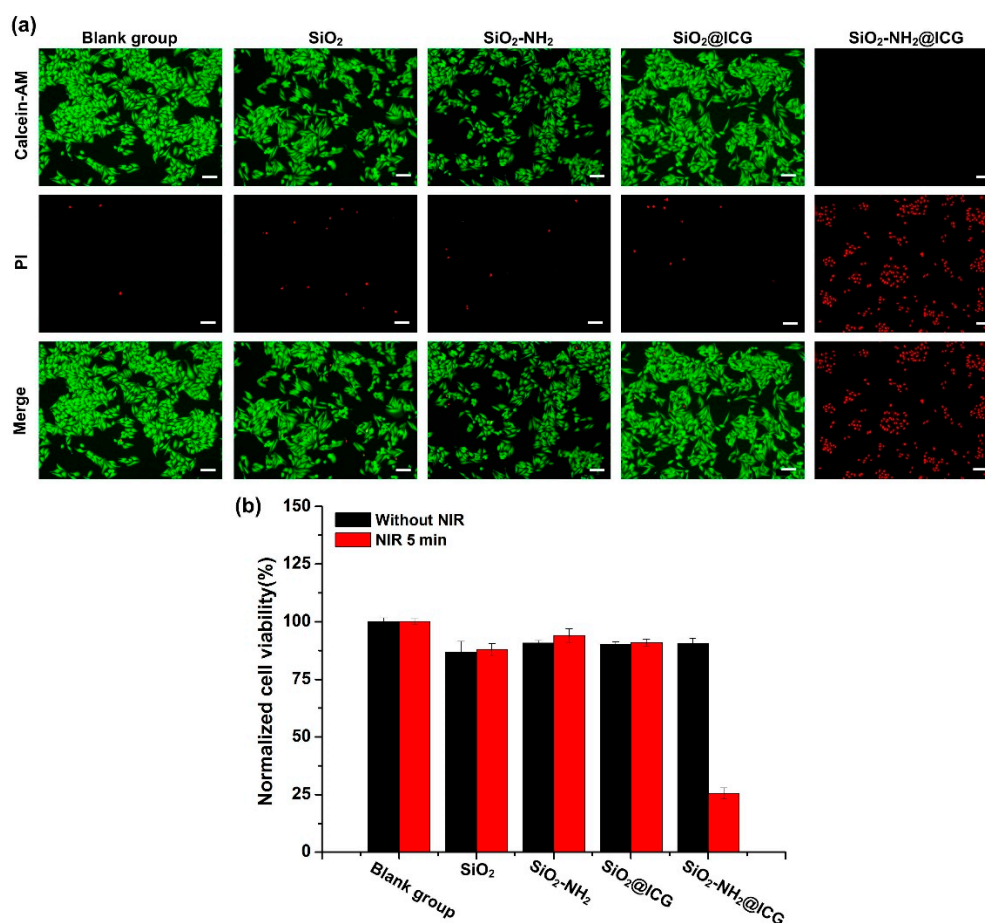


Figure 7. (a) The HepG2 cells treated with different samples media after NIR irradiation 5 min; after further 12 h culture, the cells were stained with Calcein-AM/PI fluorescent dye, scale bars, 100 μm . (b) Viability of HepG2 cells treated with SiO_2 , $\text{SiO}_2\text{-NH}_2$, $\text{SiO}_2\text{@ICG}$ and $\text{SiO}_2\text{-NH}_2\text{@ICG}$ NPs, with or without NIR irradiation (808 nm, $1.5\text{ W}/\text{cm}^2$, 5 min).

As shown in Figure 7b, all NPs groups showed high cell viability after 16 h incubation period without irradiation even at a high concentration of 200 $\mu\text{g}/\text{mL}$ (equivalent 16 $\mu\text{g}/\text{mL}$ ICG). The viability of HepG2 cells incubated with SiO_2 , $\text{SiO}_2\text{-NH}_2$, and $\text{SiO}_2\text{@ICG}$ did not change whether with a laser or not, whereas the HepG2 cells treated with $\text{SiO}_2\text{-NH}_2\text{@ICG}$ saw a sharp decrease in viability to 25%. This result confirmed that $\text{SiO}_2\text{-NH}_2\text{@ICG}$ had low cytotoxicity in HepG2 cells, but can effectively induce cell death via photothermal effects of plenty of encapsulated ICG.

3. Materials and Methods

3.1. Materials

Tetraethoxysilane (TEOS), (3-aminopropyl)-triethoxysilane (APTES), tetyl trimethylammonium bromide (CTAB), and indocyanine green (ICG) were purchased from Shanghai Aladdin Bio-Chem Technology Co. Ltd. (China). DMEM (Gibco, Grand Island, NY, USA), Trypsin (HyClone, UT, USA), Penicillin/Streptomycin (HyClone) and Fetal Bovine Serum (FBS, Gibco) were purchased from Shanghai Pufei Bio-Technology Co. Ltd. (China). Hoechst 33342 and PI Assay Kit, Annexin V-FITC and PI Assay Kit, 3-(4,5-dimethyl -2-thiazolyl)-2,5-diphenyl -2-H-tetrazolium bromide (MTT), Calcein-AM/PI Double Stain Kit and Dimethyl sulfoxide (DMSO) were purchased from Beijing Solarbio Science & Technology Co., Ltd. (China). A HepG2 cell line was provided from the American Type Culture Collection (ATCC, USA).

3.2. Synthesis of the $\text{SiO}_2\text{-NH}_2$ NPs

The amino-functionalized silica nanospheres were prepared by the sol-gel method using CTAB as a template according to the published literature [9]. Briefly, 0.279 g of CTAB was dissolved in 200 mL of DI water at 50 °C with stirring on the magnetic stirrer, and 6 mL of aqueous ammonia was added dropwise. Then, 1.394 mL TEOS was slowly added into the mixtures and stirred at 600 r/min for 4 h. Next, 0.3 mL of APTES were further introduced into the mixtures, followed with another 2 h stirring until white precipitates formed. The precipitates were washed twice with DI water and anhydrous ethanol, respectively. After cleaning, in order to remove the template (CTAB), the precipitation was refluxed at 80 °C for 36 h in acidic methanol (100 mL of methanol added to 2 mL of HCl). After reflux, the precipitates were centrifuged at 10,000 r/min for 10 min, and then, washed twice with DI water and anhydrous ethanol, respectively. Finally, the products were dried in the vacuum drying chamber overnight and recorded as $\text{SiO}_2\text{-NH}_2$ NPs. The unmodified silica nanoparticles were prepared in the same way without adding APTES and recorded as SiO_2 NPs. The final products were stored in a vacuum for further study.

3.3. Preparation of the ICG-Loaded Nanoparticles

To load ICG into the $\text{SiO}_2\text{-NH}_2$ and SiO_2 NPs, 3 mL of $\text{SiO}_2\text{-NH}_2$ NPs (5 mg/mL in water) and 3 mL ICG solution (400 $\mu\text{g}/\text{mL}$ in water) were mixed; this solution was oscillated at 25 °C at 110 r/min for 2 h. The precipitates were collected by using centrifugation at 8000 r/min for 5min and then, washed three times to remove the unloaded ICG. The ICG loaded NPs were then freeze-dried and stored in the dark. The quantity of loaded ICG was measured using an EnSpire Microplate Reader (PerkinElmer, Waltham, MA, USA) at 780 nm. The ICG LE was calculated according to Equation.

$$LE (\%) = \frac{\text{weight of loaded drug}}{\text{initial weight of drug}} \times 100 \quad (1)$$

3.4. Characterization

The morphologies of the samples were characterized using a TEM images obtained on a JEM-1200EX microscope (JEOL, Japan), operating at 120 kV. Image-Pro plus soft was used to measure the average particle size. UV-vis spectra were acquired on an EnSpire Microplate Reader. FTIR spectra

were recorded using a Nicolet 6700 IR spectrometer (Thermo Fisher, Waltham, MA, USA). Dynamic light scattering (DLS) studies were carried out using Zetasizer Nano ZS ZEN3600 (Malvern, UK) at 25 °C to analyze particle size distribution and zeta potential. The specific surface area and mesoporous pore diameter of the product were measured by nitrogen adsorption method using the ASAP 2020M specific surface area and pore size distribution analyzer (Micromeritics, Norcross, GA, USA). Thermogravimetric analysis was performed with a Netzsch STA 409 thermogravimetric analyzer (Netzsch, Germany) in the air, and the heating rate was 10 °C min⁻¹.

In order to study the release behavior of ICG from the SiO₂-NH₂@ICG and SiO₂@ICG NPs, 600 µg samples were suspended in 3 mL PBS solution (0.01 mM, pH = 6.2 and pH = 7.0) at 37 °C, respectively. At specific time points, the suspension was centrifuged to separate the NPs precipitate and the released ICG into supernatant, respectively. The absorbance of the supernatants was measured using a Microplate Reader. Three parallel samples were prepared for each group.

3.5. Measurement of the Photothermal Performance

The photothermal performance was examined by observing the temperature elevation of the different concentrations of different kinds of NPs suspension with NIR laser irradiation. Briefly, 1.0 mL of SiO₂-NH₂@ICG suspension with different concentrations (100 and 200 µg/mL) were put into a glass cuvette (optical path is 1 cm) and then, irradiated by an 808 nm high power diode laser with an output of 1.5 W/cm² for 5 min, and dimensions of the beam at the aperture were 5 × 8 mm². The temperature elevation of the solutions was recorded by a TES-1310 Thermometer (Taiwan, China) with a thermocouple microprobe submerged in the solution, while the direct irradiation of the laser on the probe was avoided. Temperature elevations of free ICG, SiO₂@ICG, SiO₂-NH₂, and SiO₂ NPs suspension with the same concentration were measured simultaneously using the same methods. A total of 1 mL of DI water was used as the blank control. The equivalent concentrations of ICG solution for 100 and 200 µg/mL SiO₂-NH₂@ICG suspension were 8 and 16 µg/mL, and these concentrations for 100 and 200 µg/mL SiO₂@ICG suspension were 1.1 and 0.55 µg/mL.

3.6. Measurement of ICG Stability Performance

3.6.1. Irradiation Stability

In total, 200 µg/mL of SiO₂-NH₂@ICG suspension were prepared; 1 mL suspension was put into a glass cuvette, and then, irradiated by an 808 nm NIR laser with an output of 1.5 W/cm² for 3 times in a cycle. The irradiation lasted for 5 min each time and the interval was 30 min. The temperature elevation of the solution was also recorded by a TES-1310 Thermometer during the experiment. The ICG solution with equivalent concentration was used as the control (16 µg/mL). The experiment was carried out in three parallel groups.

3.6.2. Thermal Stability

An amount of 200 µg/mL of SiO₂-NH₂@ICG suspension was prepared. ICG solution with equivalent concentration was used as a control (16 µg/mL). All the samples were stored in an oven at 40 °C and a fridge at 4 °C without light irradiation, respectively. After 2, 4, 6 and 8 h, 1 mL of uniform suspension was put into a glass cuvette, and then, irradiated only one time by an 808 nm NIR laser with an output of 1.5 W/cm² for 5 min; the temperature elevation of the solution was recorded by a TES-1310 Thermometer. Samples at each time point were freshly unirradiated suspensions and solutions. The experiment was carried out in three parallel groups.

3.6.3. Long-Term Stability

In total, 200 µg/mL of SiO₂-NH₂@ICG suspension and ICG solution with equivalent concentration were prepared (16 µg/mL). All the samples were kept in a 4 °C refrigerator avoiding light. At some specific time points, 1 mL was sampled in the glass cuvette, and then, irradiated by an 808 nm NIR laser

with an output of 1.5 W/cm² for 5 min, and the temperature elevation was recorded. The experiment was carried out in three parallel groups.

3.7. Hemolysis Test

A total of 1 mL fresh rabbit blood was taken and washed with 0.9% normal saline. Red blood cells were diluted with 10 mL normal saline. The NPs suspensions with different concentrations (0.1, 0.2 and 0.5 mg/mL) were prepared, and all the NPs suspension and 0.9% normal saline were kept at 37 °C for 30 min. Then, 0.2 mL of diluted red blood cells were added in 0.8 mL NPs suspension; after mixing thoroughly, the mixture was incubated at 37 °C for 60 min. Following centrifugation, the supernatant was taken and the absorbance of the supernatant at the wavelength of 570 nm was measured by a Microplate Reader. The experiment was carried out in three parallel groups. DI water was used as positive control and 0.9% normal saline as negative control. The hemolysis rate was calculated according to Equation (2):

$$\text{Hemolysisrate (\%)} = \frac{\text{OD}_{\text{sample}} - \text{OD}_{\text{negative group}}}{\text{OD}_{\text{positive group}} - \text{OD}_{\text{negative group}}} \times 100 \quad (2)$$

3.8. Cytotoxicity Assay

To investigate the cytotoxicity of SiO₂, SiO₂-NH₂, SiO₂@ICG and SiO₂-NH₂@ICG, HepG2 cells were fed regularly with DMEM media supplemented with 10% FBS and 1% streptomycin–penicillin in a humidified incubator at 37 °C and 5% CO₂. Cells were plated in 96-well tissue culture plates at a density of 1 × 10⁴ cells/well the day before experiments. Then, SiO₂, SiO₂-NH₂, SiO₂@ICG and SiO₂-NH₂@ICG suspensions were added at two kinds of concentrations (50 and 100 µg/mL) to the cells and were incubated for 24 or 96 h, respectively. Free ICG solutions with equivalent concentrations (4 and 8 µg/mL) were obtained by diluting ICG in cell culture medium. At each determined time point, cell viability was evaluated by MTT according to the manufacturer's specification. The normalized viability was denoted as the percentage of the cell viability relative to the negative control. The cells were stained with fluorescence dye (Hoechst 33342 and PI) at day 3, and then, were observed by a fluorescence microscope (Olympus, IX71, Japan).

3.9. Cell Apoptosis Assay

HepG2 cells were plated in 6-well plates at a density of 2 × 10⁵ cells per well and incubated for 24 h. Then, the cells were exposed to free ICG, SiO₂, SiO₂-NH₂, SiO₂@ICG and SiO₂-NH₂@ICG (the concentration of ICG was fixed at 8 µg/mL, and the concentration of NPs was fixed at 100 µg/mL). After incubation together for 48 h, the cells were washed with PBS several times and digested by trypsin, collected by centrifugation and washed twice. Then, the cells were resuspended in 0.5 mL of annexin-binding buffer and stained with Annexin V-FITC and PI, before testing by Flow Cytometry (Cytotflex, Beckman, Brea, CA, USA).

3.10. In Vitro Phototoxicity Testing

To determine the photothermal effect, cells were plated in 96-well polystyrene plates at a density of 1 × 10⁴ cells/well the day before experiments, then blank NPs and ICG-loaded NPs (200 µg/mL) were added to the cells and incubated for 4 h, following irradiation by an 808 nm NIR laser with an output of 1.5 W/cm² for 5 min. The cells that were incubated with the same samples for 4 h but were not under irradiation were used as the control. After another 12 h incubation, the cells were washed and stained with Calcein-AM/PI according to the manufacturer's protocol and recorded by a fluorescence microscope.

Blank NPs and ICG-loaded NPs (200 µg/mL) were incubated with cells for 4 h; the cells in the NIR-treated groups were exposed to the same 808 nm laser for 5 min. After another 12 h incubation,

the cell viabilities were evaluated using MTT assay. The normalized viability was denoted as the percentage of the cell viability relative to the negative control.

4. Conclusions

In summary, an NIR-triggered photothermal nanoparticle has been designed and prepared successfully via the modified sol–gel method, and then, through loading enough contents of ICG into SiO₂-NH₂ NPs. Due to the change of surface potential, the loading capacity of SiO₂-NH₂ NPs with positive zeta potential for ICG was greatly increased, and endowed SiO₂-NH₂@ICG NPs capable of effective photothermal conversion. Furthermore, after encapsulation of ICG, the absorption range of SiO₂-NH₂@ICG NPs in the NIR region became broader, indicating this type of nanoparticle is suitable to be used as NIR-triggered photothermal nanocarriers. As expected, under NIR irradiation, the SiO₂-NH₂@ICG NPs showed effective photothermal performance. Thanks to the protection of SiO₂-NH₂ NPs, the stability of ICG improved effectively, and the slow and continuous release of ICG from SiO₂-NH₂ NPs endowed this nanoparticle with slower decay properties and longer photothermal effect. Finally, the cytotoxicity and phototoxicity study results demonstrated the SiO₂-NH₂@ICG NPs exhibited the highest phototoxicity to HepG2 cells compared to other treatments under NIR irradiation. This study demonstrated that this NIR-triggered photothermal SiO₂-based nanoparticle could provide a potential platform for enhanced cancer cell killing.

Supplementary Materials: Supplementary Materials can be found at <http://www.mdpi.com/1422-0067/21/13/4789/s1>. The following are available online: Figure S1: TEM images of (a) SiO₂ NPs loaded ICG (average diameter is 107 nm), (b) SiO₂-NH₂ NPs loaded ICG (average diameter is 102 nm). Figure S2: FTIR spectra of ICG; Figure S3: The HepG2 cell apoptosis after treatment with (a) normal media, (b) SiO₂, (c) SiO₂-NH₂, (d) SiO₂@ICG, (e) SiO₂-NH₂@ICG NPs, (f) free ICG. ICG concentration was fixed at 8 µg/mL, NPs concentration was fixed at 100 µg/mL.; Table S1: ICG loading efficiency (LE) of SiO₂ and SiO₂-NH₂; Table S2: HepG2 cell apoptosis results.

Author Contributions: X.W. was responsible for conceptualization, data curation, funding acquisition and review; Y.W. was responsible for project administration, resources, and supervision; Y.W., C.N., S.F., and Y.L. and J.S. were responsible for formal analysis, visualization, writing, and review and editing; X.L. and Y.D. were responsible for the investigation; C.N. and Y.W. were responsible for the methodology. All authors have read and agreed to the published version of the manuscript.

Funding: This research was funded by the Major Special Projects of technological innovation of Hubei Province, China (2017ACA168) and the National Key R&D Program of China (2017YFC1103800).

Acknowledgments: Wei Wang is acknowledged for his help in TEM experiments.

Conflicts of Interest: The authors declare no conflict of interest.

References

1. Seehawer, M.; Heinzmann, F.; D'Artista, L.; Harbig, J.; Roux, P.-F.; Hoenicke, L.; Dang, H.; Klotz, S.; Robinson, L.; Doré, G. Necroptosis microenvironment directs lineage commitment in liver cancer. *Nature* **2018**, *562*, 69. [[CrossRef](#)] [[PubMed](#)]
2. Wang, X.; Zhang, A.; Sun, H. Power of metabolomics in diagnosis and biomarker discovery of hepatocellular carcinoma. *Hepatology* **2013**, *57*, 2072–2077. [[CrossRef](#)] [[PubMed](#)]
3. Fujimori, M.; Takaki, H.; Nakatsuka, A.; Uraki, J.; Yamanaka, T.; Hasegawa, T.; Shiraki, K.; Takei, Y.; Sakuma, H.; Yamakado, K. Survival with up to 10-year follow-up after combination therapy of chemoembolization and radiofrequency ablation for the treatment of hepatocellular carcinoma: Single-center experience. *J. Vasc. Interv. Radiol.* **2013**, *24*, 655–666. [[CrossRef](#)] [[PubMed](#)]
4. Kai, Y.; Huan, X.; Liang, C.; Chunyang, S.; Jun, W.; Zhuang, L. In vitro and in vivo near-infrared photothermal therapy of cancer using polypyrrole organic nanoparticles. *Adv. Mater.* **2013**, *25*, 5586–5592.
5. Cheng, L.; Yang, K.; Chen, Q.; Liu, Z. Organic stealth nanoparticles for highly effective in vivo near-infrared photothermal therapy of cancer. *ACS Nano* **2012**, *6*, 5605. [[CrossRef](#)]
6. Chen, Q.; Xu, L.; Liang, C.; Wang, C.; Peng, R.; Liu, Z. Photothermal therapy with immune-adjuvant nanoparticles together with checkpoint blockade for effective cancer immunotherapy. *Nat. Commun.* **2016**, *7*, 13193. [[CrossRef](#)]

7. Xiao, Z.; Ji, C.; Shi, J.; Pridgen, E.M.; Frieder, J.; Wu, J.; Farokhzad, O.C. DNA self-assembly of targeted near-infrared-responsive gold nanoparticles for cancer thermo-chemotherapy. *Angew. Chem. Int. Ed.* **2012**, *51*, 11853–11857. [[CrossRef](#)]
8. Rengan, A.K.; Bukhari, A.B.; Pradhan, A.; Malhotra, R.; Banerjee, R.; Srivastava, R.; De, A. In vivo analysis of biodegradable liposome gold nanoparticles as efficient agents for photothermal therapy of cancer. *Nano Lett.* **2015**, *15*, 842–848. [[CrossRef](#)]
9. Wu, L.; Wu, M.; Zeng, Y.; Zhang, D.; Zheng, A.; Liu, X.; Liu, J. Multifunctional peg modified dox loaded mesoporous silica nanoparticle@cus nanohybrids as photo-thermal agent and thermal-triggered drug release vehicle for hepatocellular carcinoma treatment. *Nanotechnology* **2015**, *26*, 025102. [[CrossRef](#)]
10. Virani, N.A.; Davis, C.; McKernan, P.; Hauser, P.; Hurst, R.E.; Slaton, J.; Silvy, R.P.; Resasco, D.E.; Harrison, R.G. Phosphatidylserine targeted single-walled carbon nanotubes for photothermal ablation of bladder cancer. *Nanotechnology* **2017**, *29*, 035101. [[CrossRef](#)]
11. Gao, S.; Zhang, L.; Wang, G.; Yang, K.; Chen, M.; Tian, R.; Ma, Q.; Zhu, L. Hybrid graphene/au activatable theranostic agent for multimodalities imaging guided enhanced photothermal therapy. *Biomaterials* **2016**, *79*, 36–45. [[CrossRef](#)] [[PubMed](#)]
12. Shao, Q.; Hu, Z.; Xu, X.; Yu, L.; Zhang, D.; Huang, Y. Mussel-inspired immobilization of bn nanosheets onto poly (p-phenylene benzobisoxazole) fibers: Multifunctional interface for photothermal self-healing. *Appl. Surf. Sci.* **2018**, *440*, 1159–1165. [[CrossRef](#)]
13. Hu, Z.; Wang, C.; Zhao, F.; Xu, X.; Wang, S.; Yu, L.; Zhang, D.; Huang, Y. Fabrication of a graphene/c 60 nanohybrid via γ -cyclodextrin host–guest chemistry for photodynamic and photothermal therapy. *Nanoscale* **2017**, *9*, 8825–8833. [[CrossRef](#)] [[PubMed](#)]
14. Kong, H.J.; Mooney, D.J. Microenvironmental regulation of biomacromolecular therapies. *Nat. Rev. Drug Discov.* **2007**, *6*, 455. [[CrossRef](#)]
15. Hu, Z.; Lu, F.; Liu, Y.; Zhao, L.; Yu, L.; Xu, X.; Yuan, W.; Zhang, Q.; Huang, Y. Construction of anti-ultraviolet “shielding clothes” on poly (p-phenylene benzobisoxazole) fibers: Metal organic framework-mediated absorption strategy. *Acs Appl. Mater. Interfaces* **2018**, *10*, 43262–43274. [[CrossRef](#)]
16. Hu, Z.; Shao, Q.; Huang, Y.; Yu, L.; Zhang, D.; Xu, X.; Lin, J.; Liu, H.; Guo, Z. Light triggered interfacial damage self-healing of poly (p-phenylene benzobisoxazole) fiber composites. *Nanotechnology* **2018**, *29*, 185602. [[CrossRef](#)] [[PubMed](#)]
17. Schütt, F.; Fischer, J.; Kopitz, J.; Holz, F.G. Indocyanine green angiography in the presence of subretinal or intraretinal haemorrhages: Clinical and experimental investigations. *Clin. Exp. Ophthalmol.* **2002**, *30*, 110–114. [[CrossRef](#)] [[PubMed](#)]
18. Fickweiler, S.; Szeimies, R.-M.; Bäuml, W.; Steinbach, P.; Karrer, S.; Goetz, A.E.; Abels, C.; Hofstädter, F. Indocyanine green: Intracellular uptake and phototherapeutic effects in vitro. *J. Photochem. Photobiol. B Biol.* **1997**, *38*, 178–183. [[CrossRef](#)]
19. Quan, B.; Choi, K.; Kim, Y.-H.; Kang, K.W.; Chung, D.S. Near infrared dye indocyanine green doped silica nanoparticles for biological imaging. *Talanta* **2012**, *99*, 387–393. [[CrossRef](#)]
20. Wishart, G.; Loh, S.-W.; Jones, L.; Benson, J. A feasibility study (icg-10) of indocyanine green (icg) fluorescence mapping for sentinel lymph node detection in early breast cancer. *Eur. J. Surg. Oncol. (Ejso)* **2012**, *38*, 651–656. [[CrossRef](#)]
21. Saxena, V.; Sadoqi, M.; Shao, J. Degradation kinetics of indocyanine green in aqueous solution. *J. Pharm. Sci.* **2003**, *92*, 2090–2097. [[CrossRef](#)] [[PubMed](#)]
22. Desmettre, T.; Devoisselle, J.; Mordon, S. Fluorescence properties and metabolic features of indocyanine green (icg) as related to angiography. *Surv. Ophthalmol.* **2000**, *45*, 15–27. [[CrossRef](#)]
23. Yaseen, M.A.; Yu, J.; Wong, M.S.; Anvari, B. Laser-induced heating of dextran-coated mesocapsules containing indocyanine green. *Biotechnol. Prog.* **2007**, *23*, 1431–1440. [[CrossRef](#)] [[PubMed](#)]
24. Zheng, C.; Zheng, M.; Gong, P.; Jia, D.; Zhang, P.; Shi, B.; Sheng, Z.; Ma, Y.; Cai, L. Indocyanine green-loaded biodegradable tumor targeting nanoprobes for in vitro and in vivo imaging. *Biomaterials* **2012**, *33*, 5603–5609. [[CrossRef](#)]
25. Hong, S.H.; Kim, H.; Choi, Y. Indocyanine green-loaded hollow mesoporous silica nanoparticles as an activatable theranostic agent. *Nanotechnology* **2017**, *28*, 185102. [[CrossRef](#)]

26. Wang, W.; Zhao, Y.; Yan, B.-B.; Dong, L.; Lu, Y.; Yu, S.-H. Calcium carbonate-doxorubicin@silica-indocyanine green nanospheres with photo-triggered drug delivery enhance cell killing in drug-resistant breast cancer cells. *Nano Res.* **2018**, *11*, 3385–3395. [[CrossRef](#)]
27. Li, A.; Wang, Y.; Chen, T.; Zhao, W.; Zhang, A.; Feng, S.; Liu, J. Nir-laser switched icg/dox loaded thermo-responsive polymeric capsule for chemo-photothermal targeted therapy. *Eur. Polym. J.* **2017**, *92*, 51–60. [[CrossRef](#)]
28. Lee, C.H.; Cheng, S.H.; Wang, Y.J.; Chen, Y.C.; Chen, N.T.; Souris, J.; Chen, C.T.; Mou, C.Y.; Yang, C.S.; Lo, L.W. Near-infrared mesoporous silica nanoparticles for optical imaging: Characterization and in vivo biodistribution. *Adv. Funct. Mater.* **2009**, *19*, 215–222. [[CrossRef](#)]
29. Lei, Q.; Qiu, W.X.; Hu, J.J.; Cao, P.X.; Zhu, C.H.; Cheng, H.; Zhang, X.Z. Multifunctional mesoporous silica nanoparticles with thermal-responsive gatekeeper for nir light-triggered chemo/photothermal-therapy. *Small* **2016**, *12*, 4286–4298. [[CrossRef](#)]
30. Lv, R.; Wang, D.; Xiao, L.; Chen, G.; Xia, J.; Prasad, P.N. Stable icg-loaded upconversion nanoparticles: Silica core/shell theranostic nanopatform for dual-modal upconversion and photoacoustic imaging together with photothermal therapy. *Sci. Rep.* **2017**, *7*, 15753. [[CrossRef](#)]
31. Shindo, Y.; Inose, T.; Kubota, Y.; Oikawa, T.; Tokunaga, M.; Kamei, T.; Gonda, K.; Kobayashi, Y. Synthesis on aggregation of colloidal solutions of icg-active silica nanoparticles and their application in in-vivo fluorescence imaging. *Mater. Chem. Phys.* **2018**, *220*, 201–207. [[CrossRef](#)]
32. Palanikumar, L.; Choi, E.S.; Cheon, J.Y.; Joo, S.H.; Ryu, J.H. Noncovalent polymer-gatekeeper in mesoporous silica nanoparticles as a targeted drug delivery platform. *Adv. Funct. Mater.* **2015**, *25*, 957–965. [[CrossRef](#)]
33. Ilhan-Ayisigi, E.; Yesil-Celiktas, O. Silica-based organic-inorganic hybrid nanoparticles and nanoconjugates for improved anticancer drug delivery. *Eng. Life Sci.* **2018**, *18*, 882–892. [[CrossRef](#)]
34. Mitragotri, S.; Burke, P.A.; Langer, R. Overcoming the challenges in administering biopharmaceuticals: Formulation and delivery strategies. *Nat. Rev. Drug Discov.* **2014**, *13*, 655–672. [[CrossRef](#)] [[PubMed](#)]
35. Wang, H.; Li, X.; Tse, B.W.-C.; Yang, H.; Thorling, C.A.; Liu, Y.; Touraud, M.; Chouane, J.B.; Liu, X.; Roberts, M.S. Indocyanine green-incorporating nanoparticles for cancer theranostics. *Theranostics* **2018**, *8*, 1227. [[CrossRef](#)]
36. Tang, F.; Li, L.; Chen, D. Mesoporous silica nanoparticles: Synthesis, biocompatibility and drug delivery. *Adv. Mater.* **2012**, *24*, 1504–1534. [[CrossRef](#)] [[PubMed](#)]
37. He, Q.; Shi, J. Mesoporous silica nanoparticle based nano drug delivery systems: Synthesis, controlled drug release and delivery, pharmacokinetics and biocompatibility. *J. Mater. Chem.* **2011**, *21*, 5845–5855. [[CrossRef](#)]
38. Serra, J.; González, P.; Liste, S.; Serra, C.; Chiussi, S.; León, B.; Pérez-Amor, M.; Ylänen, H.; Hupa, M. Ftir and xps studies of bioactive silica based glasses. *J. Non-Cryst. Solids* **2003**, *332*, 20–27. [[CrossRef](#)]
39. Sun, Y.; Zhang, Z.; Wong, C. Study on mono-dispersed nano-size silica by surface modification for underfill applications. *J. Colloid Interface Sci.* **2005**, *292*, 436–444. [[CrossRef](#)]
40. Weigand, R.; Rotermund, F.; Penzkofer, A. Aggregation dependent absorption reduction of indocyanine green. *J. Phys. Chem. A* **1997**, *101*, 7729–7734. [[CrossRef](#)]
41. Li, L.; Liu, Y.; Hao, P.; Wang, Z.; Fu, L.; Ma, Z.; Zhou, J. Pedot nanocomposites mediated dual-modal photodynamic and photothermal targeted sterilization in both nir i and ii window. *Biomaterials* **2015**, *41*, 132–140. [[CrossRef](#)] [[PubMed](#)]
42. Li, H.; Li, J.; Ke, W.; Ge, Z. A near-infrared photothermal effect-responsive drug delivery system based on indocyanine green and doxorubicin-loaded polymeric micelles mediated by reversible diels–alder reaction. *Macromol. Rapid Commun.* **2015**, *36*, 1841–1849. [[CrossRef](#)] [[PubMed](#)]
43. Sheng, Z.; Hu, D.; Xue, M.; He, M.; Gong, P.; Cai, L. Indocyanine green nanoparticles for theranostic applications. *Nano-Micro Lett.* **2013**, *5*, 145–150. [[CrossRef](#)]

